Characterizing stress corrosion cracking in stainless steel using nonlinear resonant ultrasound spectroscopy

Stephen M. Hogg

A senior thesis report submitted to the faculty of

Brigham Young University

In partial fulfillment of the requirements for the degree of

Bachelor of Science

Brian E. Anderson, Advisor

Department of Physics and Astronomy

Brigham Young University

June 2018

ABSTRACT

Characterizing stress corrosion cracking in stainless steel using nonlinear resonant ultrasound spectroscopy

Stephen M. Hogg

Department of Physics and Astronomy

Bachelor of Science

Spent nuclear fuel rods are stored in stainless steel containers and may be stored for decades. In order prevent radiation leakage, the stainless steel structure must not be compromised. These containers are susceptible to stress corrosion cracking (SCC). Traditional nondestructive evaluation methods have been developed to detect open cracks but these cannot detect the closed portion of the crack that may extend further. Nonlinear Resonant Ultrasound Spectroscopy (NRUS) is used here to determine if it can be used to quantify a cumulative amount of SCC in a structure. To induce SCC in a timely manner, cylindrical, 304L stainless steel rods are immersed in a heated 42% magnesium chloride solution. A set of rods are removed one by one after different lengths of exposure to the hot magnesium chloride solution. NRUS measurements are then conducted on longitudinal modes in the rods. Rods exposed longer did indeed result in a larger resonance frequency shift, and therefore a larger nonlinear parameter, α, in NRUS measurements. It is observed that α can be used to detect SCC before visible cracks appear on the rods.

Keywords: Nondestructive Evaluation, Nondestructive Testing, Nonlinear Resonant Ultrasound, Stress Corrosion Cracking.

Acknowledgments

Many people helped me to get the research to this point as well as helping me become who I am today. I would like to acknowledge Dr. Kara Stowers from the Brigham Young University Department of Chemistry and Biochemistry for allowing us to use her lab as a space to damage samples. I would also like to acknowledge financial support through a subcontract from Los Alamos National Laboratory, the Brigham Young University College of Physical and Mathematical Sciences, and the Brigham Young University Department of Physics and Astronomy.

Many thanks go out to my advisor Dr. Anderson for his patient tutelage and who has put in many hours of work into this thesis and has been instrumental in my growth as a physicist. I would like to thank my parents Merrill and Lisa Hogg for all of the care and support that they have given and for helping me to try harder to do better. Above all, many thanks to my wife and dear companion Heather for being a stalwart partner and for acting as a sounding board when I needed it.

Table of Contents

List of Figures

List of Tables

Chapter 1 Introduction

Nondestructive evaluation (NDE) methods are needed to characterize damage on 304L stainless steel nuclear storage casks. Great care must be taken with nuclear storage casks because they contain radioactive particles. Damage, specifically the development of cracking, on these casks may eventually lead to containment breaches, causing a public health hazard, therefore damage needs to be characterized.[1] One of the main types of damage possible in the steel used for nuclear storage casks is Stress Corrosion Cracking (SCC). SCC occurs when a stress is applied to a metal, including residual stresses that arise in welding, and the metal is in a corrosive environment (including airborne chlorides).[1] On the microscopic scale the metal and the corrosive environment result in an electrochemical reaction. Over time, this reaction will crack the metal. Since most of the nuclear storage casks are close to an ocean and are therefore in an environment with a high percentage of airborne chlorides, SCC is an important potential type of damage to characterize.

SCC is most likely to occur in an area known as the Heat Affected Zone (HAZ). HAZs are created during the welding process. Because of the intense heat of the welding process, the material properties and grain boundaries within the HAZ are changed.[2] Not only does this affect the strength of the metal but this can also degrade the metal's capacity to resist corrosion, making it much more likely for SCC to occur. It should be noted that SCC damage can be incredibly small. It may be small enough that visual techniques and even linear NDE techniques may not be able to detect it. Linear NDE techniques often rely on a reflection of sound off of a feature, but if the crack is too small or is a closed crack with the crack surfaces in contact, then no reflection will occur. Nonlinear NDE techniques, on the other hand, are well suited to detect closed cracks because surfaces in contact with one another vibrate nonlinearly.[3] Given the fact that these cracks are likely to appear next to welds, it is imperative that a nonlinear NDE method is used to characterize the damage. SCC may eventually break through the thickness of the cask, allowing radiation to leak out. Therefore SCC should be detected early on so that preventative measures can be implemented.

One type of nonlinear effect of interest here is that of the amplitude dependence of resonance frequencies of a damaged sample. Young's modulus is strain independent for linear elastic materials, but in damaged, nonlinear materials it depends on the strain experienced by the material. If we strike a damaged steel rod with a hammer harder and harder, a progressively lower frequency tone will be emitted.[4] Nonlinear elasticity is the reason behind this phenomenon. Inducing a higher strain will lower the Young's modulus of the sample according to the following equation derived by Remillieux *et al.*,[5]

$$E(x) = E_0[1 - \alpha_E \varepsilon_{xx}^{\max}(x)] \quad (1)$$

where $E(x)$ is amplitude dependent Young's Modulus, E_0 is the undamaged Young's modulus

of the bulk material, and $\varepsilon_{xx}^{\max}$ is the maximum strain measured in the longitudinal direction during a longitudinal mode of vibration. Here α_E is a nonclassical nonlinear elastic parameter that has been correlated with inhomogeniety. For instance, freshly milled stainless steel will have a very low, almost zero, α_E. A sedimentary rock, such as sandstone, will have a much larger α_E. Damaged materials will also exhibit a measurable α_E.

Nonlinear Resonant Ultrasound Spectroscopy (NRUS) is a technique used to measure the α_E of a sample.[6] NRUS is used to measure the amplitude dependence of a particular mode's resonance frequency. A swept sine wave excitation signal, starting from a frequency below the expected resonance frequency to a frequency above the resonance frequency, is used to extract the resonance frequency. The amplitude of the excitation signal is then increased several times and the resulting resonance frequency noted each time. A shift downward in the resonance frequency with increasing strain amplitude is often encountered for damaged media as the elastic modulus softens (as implied in Eq. (1)). The strain at the resonance frequency peak is also extracted as a function of input excitation. The slope of a plot of the relative frequency shift as a function of strain determines α_E for the sample.[6]

NRUS was originally developed at Los Alamos National Laboratory in the 1990's in order to characterize the nonlinearity of a sample.[4] It was initially developed to study rock samples and has been used to study sandstone, soapstone, and granite.[7] It has been applied to characterize damage in materials that otherwise exhibit no NRUS shift, such as fatigue damage in copper and creep damage in stainless steel .[8,9] Additionally it has been applied to characterize damage in materials that exhibit a NRUS shift in their undamaged state but the shift, and therefore the α_E, increase further due to the presence of damage in order to characterize thermal damage in concrete and damage in bone.[10,11,12]

Various nonlinear acoustic techniques have been used to detect and characterize SCC, including the following. Ohara *et al.* developed the Subharmonic Phased Array for the detection of SCC on the opposing surface of a metal sample and on the same side as the array using surface acoustic waves.[13,14] Dynamic Acousto-Elastic Testing is a low frequency pump and higher frequency probe technique that was used by Rivière *et al*. to extract α_E and additional nonlinear parameters.[15] Ohara *et al*. used NRUS to locate SCC by analyzing the measured α_E from a couple different resonance modes based on whether the mode had a strain node or antinode at the location of the SCC.[16] An experiment by Morlock *et al*. used nonlinear Rayleigh surface waves to characterize SCC on four samples with different amounts of SCC.[17] These samples were exposed to the same corrosive environment for the same exposure time but each was exposed to different amounts of applied stress. Anderson *et al.* used the Time Reversed Elastic Nonlinearity Diagnostic to explore the depth dependence of SCC near welds.[18] The majority of the nonlinear acoustic techniques were applied to a single sample for proof of concept of the technique's ability to detect SCC rather than being applied to a set of samples with progressive damage.

The purpose of this thesis is to characterize overall SCC damage in 304L stainless steel samples by measuring α_E. Samples are placed in a hot magnesium chloride ($MgCl_2$) bath for varying lengths of time to induce SCC. It will be shown that α_E in progressively damaged samples does increase with the amount of damage induced and that NRUS can therefore quantify the damage by measuring the α_E.

Chapter 2 Experimental Methods

2.1 Sample Creation

Samples of 304L stainless steel having a weld and a cylindrical shape are created. The simple geometry of the cylindrical shape ensures that individual modes may be identified and excited. The weld provides a HAZ where SCC would most likely develop. The actual samples are created by welding two 6.35 cm (2.5 in.) length pieces to create 12.7 cm (5 in.) long samples. The weld material is 308 stainless steel, which is the same weld material used on the nuclear storage casks. Figure 4 displays a photograph of some of the virgin samples with the weld and HAZ identified. Visually the samples appear to have been welded similarly.

FIG. 1 Photograph of five of the samples before inducing damage. Also depicted are the weld region and the Heat Affected Zone (HAZ).

The process for inducing SCC consists of placing the samples in a hot, corrosive environment to accelerate the rate of the development of cracking. The environment consists of a 42% $MgCl_2$ solution created by mixing tap water with anhydrous $MgCl_2$. The beaker used to contain the solution has a total volume of 1 L and is filled on average to the 500 mL mark. The solution is maintained at 80º C using a hot plate for the duration of the exposure of the rods to the solution. Since the solution is at a high temperature, evaporation occurs, necessitating refilling the beaker. The amount of solution refill needed is reduced by using a watch glass to mostly cover the beaker, allowing evaporated water to condense on the watch glass and drip back down into the solution. Only water is needed to restore the $MgCl_2$-water ratio, since only the

water evaporates. Adding additional $MgCl_2$ will cause the solution to be oversaturated. When samples are removed, $MgCl_2$ and water are added to maintain the 42% solution since some salt adheres to the rod surface and needs to be replaced. Twelve samples are placed in the solution and then one is taken out every two days.

FIG. 2. Photograph of some of the samples in the hot magnesium chloride solution in a fume hood.

2.2 Experimental Setup

NRUS experiments are controlled and data are taken using custom LabVIEW software. The software sends out a stepped sine wave signal through a National Instruments (Austin, TX) PXI-5406 FGEN card (16-bit resolution and 40 MHz sampling frequency). This signal is amplified using a Tabor Electronics (Nesher, Israel) Amplifier, model 9400 with a fixed 50 times

gain. The amplified signal is send to a cylindrical, APC International (Mackeyville, PA) piezoelectric transducer of type 851, with dimensions 15.7 mm diameter by 6.4 mm thickness. As the sample is excited by a quasi-continuous wave with the transducer, the response is measured by a Polytec (Waldbronn, Germany) PSV-400 Scanning Laser Doppler Vibrometer (SLDV), whose output is digitized with a National Instruments PXIe-5122 digitizer (14-bit resolution and 100 MHz sampling frequency). Figure 6 depicts how the experimental apparatus is set up. As shown in Fig. 6, the laser is shined on the end of the sample that does not have a piezoelectric transducer (PZT) attached.

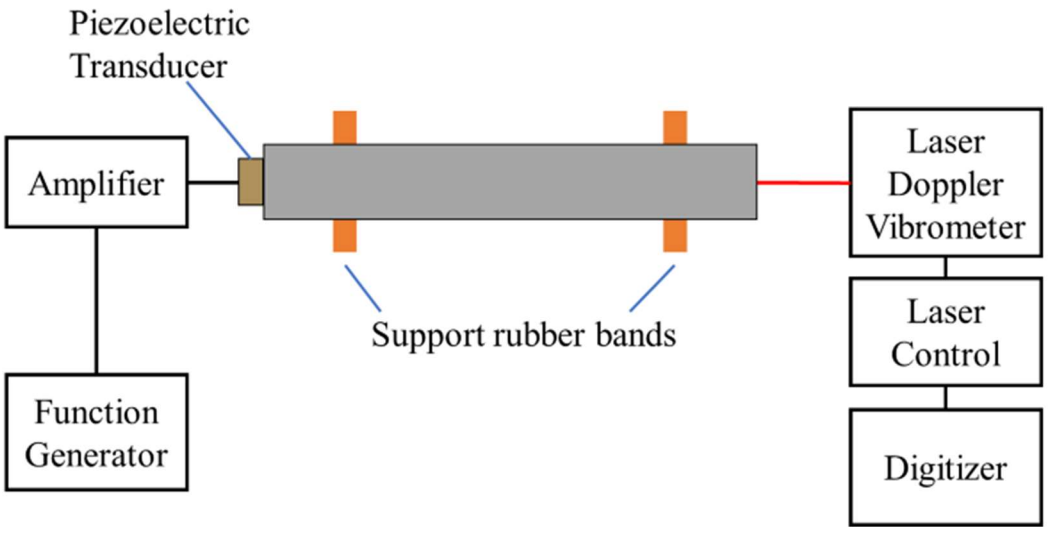

FIG. 3. Diagram of the experimental setup to use nonlinear resonant ultrasound spectroscopy on the sample under test.

As mentioned previously, the software used to control the experiments and acquire data is a custom software developed and licensed by Los Alamos National Laboratory called Resonance Inspection Techniques & Analyses (RITA). The five major settings in the RITA software are:

frequency resolution, frequency range, ring-up time, acquisition time, and voltage amplitudes. During measurements, RITA sends a stepped sine voltage signal to the amplifier as outlined previously. This signal consists of a sine wave that lasts for the duration of the specified ring-up and acquisition times (allowing for transient ring up and steady state portions of the excitation of the sample). RITA repeats this process for each frequency within the specified frequency range and resolution. This process is then repeated at each specified voltage amplitude.

The frequency range of the stepped sine wave excitation is selected to excite the first longitudinal mode of vibration of the sample. This sample can be modeled as having a mass loaded end (with the piezoelectric transducer as the mass load) and a free end. The assumed time-harmonic solution to the longitudinal wave equation is

$$\boldsymbol{\xi}(x) = [\boldsymbol{A}\cos(kx) + \boldsymbol{B}\sin(kx)]e^{j\omega t}. \tag{2}$$

By applying the boundary condition $\left(\frac{\partial \xi}{\partial x}\right)_{x=0} = 0$, the expression turns into

$$\boldsymbol{\xi}(x) = \boldsymbol{A}\cos(kx)e^{j\omega t}. \tag{3}$$

Since the longitudinal vibrations will accelerate the mass, the boundary condition for $x = L$ is $\boldsymbol{f}_L = m(\partial^2\xi/\partial t^2)_{x=L}$, where $\boldsymbol{f}_L$ is the restoring force presented to the end of the rod and can be expressed as $\boldsymbol{f}_L = -SE(\partial\xi/\partial x)_{x=L}$, where S is the cross sectional area and E is the Young's modulus. Setting these two forces equal to each other results in

$$-SE\left(\frac{\partial \xi}{\partial x}\right)_{x=L} = m\left(\frac{\partial^2 \xi}{\partial t^2}\right)_{x=L}, \tag{4}$$

which can be further simplified to

$$\tan(kL) = -\frac{m\omega c}{SE}. \quad (5)$$

By replacing *E* with the product of the density and the squared longitudinal speed of sound, ρc^2, and equating the mass of the bar, m_b, with ρSL, Eq. (5) becomes

$$\tan(kL) = -(m/m_b)kL. \quad (6)$$

This transcendental equation is used to predict the longitudinal resonances in Table 1.[19,20,21] Since the samples are of length 12.7 cm (5 in.) and diameter 1.59 cm (5/8 in.) they are found to have longitudinal modes that are widely separated from torsional and flexural modes as shown in Table I.[22]

TABLE 1. Predicted resonance frequencies of a 12.7 cm length, 1.59 cm diameter rod made of 304L stainless steel. The torsional and bending modes assume a free-free rod, whereas the longitudinal modes utilize the free-mass loaded rod expression developed in Eq. (6). Measured longitudinal modes are also given.

Mode Number	Torsional Modes (kHz)	Bending Modes (kHz)	Longitudinal Modes (kHz)	Measured Longitudinal Modes (kHz)
1	10.7	3.75	18.0	18.4
2	21.5	10.3	36.1	38.8
3	32.2	20.2	54.1	46.1

Chapter 3 Results

NRUS data are taken with a frequency resolution of 0.2 Hz. The frequency range used depends on the resonance frequency of the sample under test. Relatively undamaged samples have a frequency range that is slightly wider than the full width at half maximum span of frequencies. More damaged samples require a wider frequency range that extends further below the sample's resonance frequency, because the frequency shift is greater in damaged samples. The sample exposed for the longest time, which is expected to have the most damage, is measured from 14.8-15.4 kHz while the undamaged sample was measured from 18.2-18.5 kHz. The NRUS measurements utilize excitation voltage levels of 10V-100V in increments of 10V output from the amplifier to the transducer.

Figure 4 displays sample NRUS measurements from samples exposed for 6 days, 14 days, and 22 days. Once the NRUS data is obtained, a parabolic peak-finding algorithm is used in the RITA software to carefully identify the peaks of the resonance curves (minimizing noise in the measured peaks), including the frequency at which the peak occurs and the amplitude of the

peak. The measured peak amplitudes and resonance frequencies are exported to MATLAB to apply linear curve fitting (see Appendix A for code) in order to extract the α_E of the sample. The relative frequency shift is defined as

$$\frac{\Delta f}{f_0} = \frac{(f_i - f_0)}{f_0}, \tag{2}$$

where f_i is the measured resonance frequency (obtained from the RITA peak-finding algorithm) at the *i*th excitation amplitude and f_0 is the lowest amplitude resonance frequency measured. The strain for each resonance curve is calculated by dividing the peak velocity measured (obtained from the RITA peak-finding algorithm) by the sample's longitudinal sound speed.[5] The relative frequency shift values are plotted as a function of the strain and these data are analyzed in MATLAB using a least squares linear fit to extract the slope of the data. The absolute value of the slope is the measured α_E. Figure 5 displays three sets of relative frequency shift data as a function of strain for the NRUS results displayed in Fig. 4 along with the linear fit to each data set. The measured α_E are 5.80 x 10^{-4}, 2.47 x 10^{-3}, and 1.03 x 10^{-2}, respectively. The respective coefficient of determination, R^2, values were 0.983, 0.984, and 0.991.

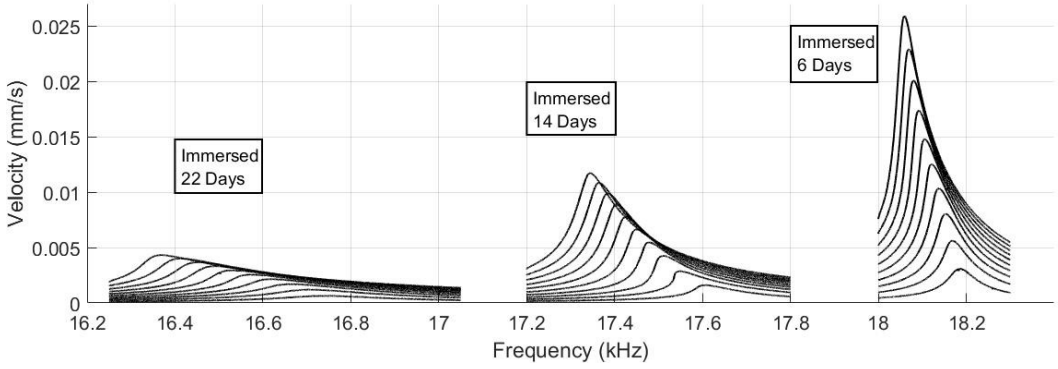

FIG. 4. Sample nonlinear resonant ultrasound spectroscopy plots from three samples exposed to hot magnesium chloride for 6, 14, and 22 days in (a), (b), and (c) respectively, showing the amplitude dependence of the first longitudinal mode frequency.

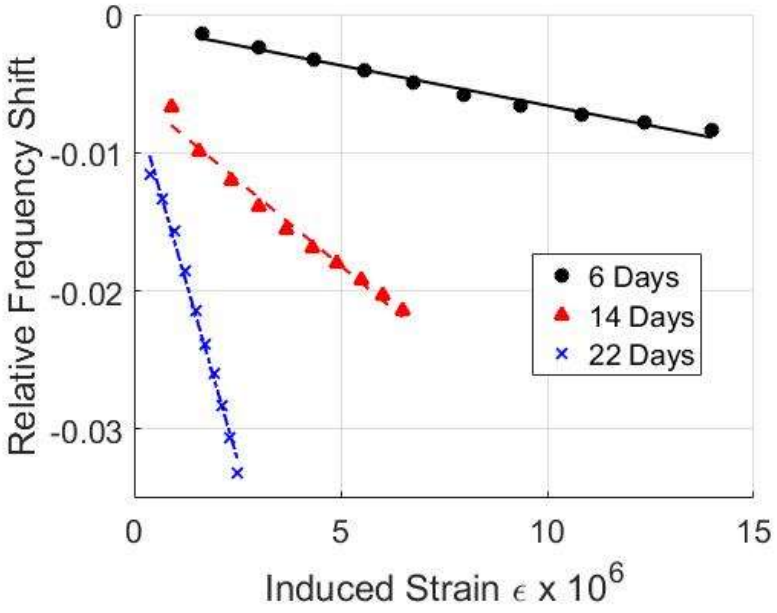

FIG. 5. Relative frequency shift, $(f_i - f_0)/f_0 = \Delta f/f_0$, as a function of induced strain, ϵ, for three samples tested. f_0 is the low amplitude resonance frequency and f_i is the resonance frequency measured for the *i*th excitation level. Included are dashed lines which indicate the linear fits for the measurements.

The process outlined above is followed for 13 samples. Table 2 displays the measured quality factor for the lowest amplitude excitation resonance curve, the effective Young's modulus calculated using Eq. (6) and the lowest amplitude resonance frequency, the maximum frequency shift measured at the highest excitation level, the maximum strain induced, the measured α_E, and the R^2 of the linear fit for every sample. Figure 6 plots α_E as a function of time exposed to $MgCl_2$. It should be noted that while there is not a consistent monotonic increase, α_E appears to increase exponentially with a longer exposure time.

Table 2. Results given for experiments conducted on 13 samples. The quality factor and Young's modulus are measured during a low level excitation. There is a general increase in α_E as the days exposed to $MgCl_2$ increases.

Days Exposed	Quality Factor	Young's Modulus (GPa)	Max $\frac{\Delta f}{f_0}$ (x 10^3)	Max Strain ($\mu\epsilon$)	α_E (x 10^3)	R^2
0	455	175	0.48	25.9	0.0217	0.909
2	460	176	0.31	23.9	0.00926	0.830
4	473	175	0.44	24.7	0.00771	0.651
6	298	171	8.37	14.0	0.581	0.983
8	138	162	10.5	4.20	1.69	0.999
10	294	162	5.56	11.6	0.314	0.949
12	152	161	10.3	5.23	1.97	0.994
14	182	163	21.5	6.50	2.48	0.984
16	166	164	21.5	5.70	3.71	0.987
18	234	158	22.1	6.50	2.17	0.999
20	242	166	13.4	7.05	1.96	0.879
22	74.6	149	33.2	2.51	1.03	0.991
24	103	121	26.8	2.40	7.50	0.955

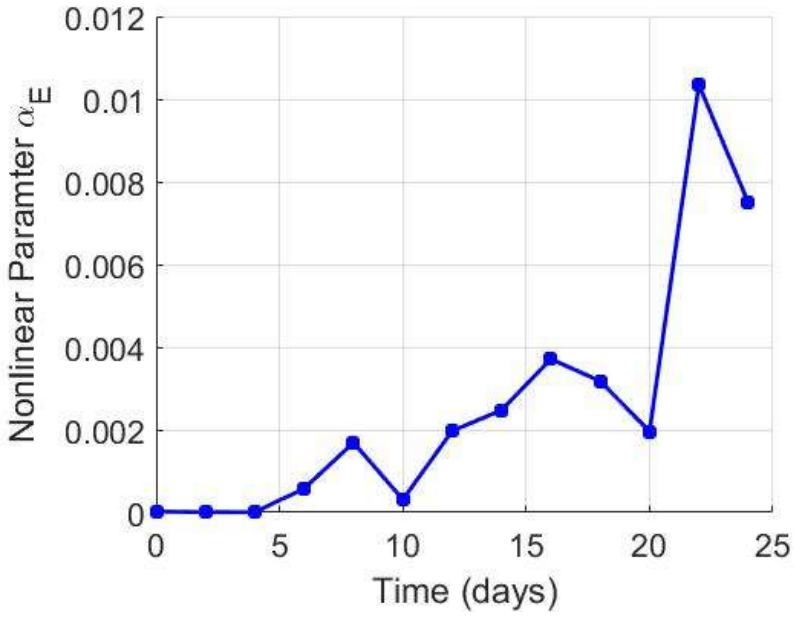

FIG. 6. The measured nonlinearity parameter, α_E, as a function of exposure time for the samples tested. The trend is generally an exponential increase in α_E with time.

Several assumptions were made that could account for discrepancies in the data. It was assumed that the welds on the rods were identical with identical rod geometries. Differences in the welding process for each sample can result in corresponding differences in residual stresses induced during the welding. Different residual stresses in the rods could easily result in damage induced at different rates since the difference in HAZs (e.g. greater variability in grain boundaries) would mean that certain rods would be more susceptible to SCC. Another assumption is that the laser of the SLDV is pointed perpendicular to the sample and that the samples are supported by the rubber bands in the same way. It was also assumed that the piezoelectric transducers are the same and that they were bonded to the samples in the same manner. If this assumption weren't true, each bar would have different excitation amplitudes, resulting in different strain measurements which affects the measured α_E. Care was taken to avoid variation in each of the above experimental conditions.

Chapter 4 Conclusion

Twelve stainless steel samples have been exposed to hot magnesium chloride for different lengths of time ranging from 2 days to 24 days to induce Stress Corrosion Cracking (SCC) in an accelerated manner. Nonlinear Resonant Ultrasound Spectroscopy (NRUS) was used to measure the amplitude dependence of the first longitudinal resonance frequency of the samples. The nonlinear parameter, α_E, was extracted from the relative shifting of the resonance frequencies, measured as a function of assumed strain levels. It was found that SCC can be induced in a relatively fast manner using lower temperatures than typically used in the literature.[23] It was also found that while there is not a perfect monotonic increasing trend, there still is a general exponential trend between exposure time and the measured α_E, which shows that NRUS can detect a likely cumulative degree of SCC in a sample. Differences in the data are thought to be due to differences in the welding process when the samples were created. Given the assumptions made, the trend shown in Fig. 6 indicates that higher quantities of SCC damage exhibit larger nonlinear shifts in resonance frequency.

Appendix A

The following code was used to calculate α_E and to create most of the graphs used in this thesis. The NRUS data has three parts. One column that has the frequency data, and two columns for each excitation level that contains the real and imaginary parts of the data. Multiple loops are used to plot the data. The other important data are the .pks files exported from RITA. These files include the peak frequencies, heights, and widths. The frequencies and their respective widths are useful for calculating the quality factor. The frequencies and peak heights are instrumental in calculating α_E. The process is to first find the frequency of the low level excitation to use as the base frequency. The measured peak heights are then converted from the RITA amplitude to the induced strain. The rest of the process is outlined in chapter 3.

```
set(0,'DefaultAxesFontSize',24); %often 28  for paper,  32  for presentation
set(0,'DefaultAxesFontWeight','demi') %often demi   for paper,  bold    for
talk
set(0,'DefaultAxesLineWidth',2); %often 2   for paper,  4 for   presentation
set(0,'DefaultLineLineWidth',4); %often 4 for   paper,  8   for talk
set(0,'DefaultFigurePosition',[20 50    1200    600])
%%
clear; close all;
set(0,'DefaultLineLineWidth',4);
num = 26;
```

```
A=zeros(6201,21,num);
P=zeros(4,40,num);
avg = 0;
for n=1:1:num
    a=dlmread(sprintf('June_12/June_12-scan%d.dat',n),' ',1,0);
    A(1:size(a,1),1:size(a,2),n) = a;
    p =dir(sprintf('June_12/June_12-scan%d-scan%d.pks',n));
    if isequaln(size(p,1),0)
        p=dlmread(sprintf('June_12/June_12-scan%d.pks',n),'\t',1,0);
        P(1:size(p,1),1:size(p,2),n)= p;
    end
end
for n = 2:2:num
    figure
    hold on
    m=1;
    q(n/2)=P(1,1,n)/P(1,2,n);
    data = abs(A(:,2,n) + 1i*A(:,3,n));
    frontf = find(A(:,1,n),1,'first');
    backf = find(A(:,1,n),1,'last');
    fr = find(data,1,'first');
    ba = find(data,1,'last');
    plot(A(frontf:backf,1,n)./1000,data(fr:ba).*4./50,'k')
        for u = 2:1:10
            data = abs(A(:,2*u,n) + 1i*A(:,2*u +1,n));
             avg = [avg mean(data(fr:ba))];
            plot(A(frontf:backf,1,n)./1000,data(fr:ba).*4./50,'k');
        end
        title(sprintf('%d Days Damaged',(n-2)),'fontsize',16);
        grid;
        xlabel('Frequency (kHz)','fontsize',18)
        ylabel('Velocity (mm/s)','fontsize',18)
        set(gca,'fontsize',16)
        f0= P(1,1,n-1);
        lambda = 2*5*.0254;
        c(n/2)= lambda*f0;
        for u=1:1:10
            b(n/2,u) = P(1,4*u -1,n);
            f(n/2,u) = P(1,4*u -3,n);
            g(n/2,u) = (f(n/2,u)-f0)/f0;
        end

    hold off
end
figure
hold on
for n=1:1:3
    if n==1
        temp = 8;
    end
    if n ==2
        temp = 16;
    end
    if n==3
        temp =24;
    end
    data = abs(A(:,2,temp) + 1i*A(:,3,temp));
```

```
    frontf = find(A(:,1,temp),1,'first');
    backf = find(A(:,1,temp),1,'last');
    fr = find(data,1,'first');
    ba = find(data,1,'last');
    plot(A(frontf:backf,1,temp)./1000,data(fr:ba).*4./50,'k-')
    for u = 2:1:10
        data = abs(A(:,2*u,temp) + 1i*A(:,2*u +1,temp));
        avg = [avg mean(data(fr:ba))];
        plot(A(frontf:backf,1,temp)./1000,data(fr:ba).*4./50,'k-');
    end
    grid;
    xlabel('Frequency (kHz)','fontsize',18)
    ylabel('Velocity (mm/s)','fontsize',18)
    set(gca,'fontsize',16)
end
hold off
eps=zeros(num/2,10);
for n=1:1:num/2
    for m=1:1:10
        eps(n,m) = b(n,m)./5./c(n).*1e6;
    end
end
eps(13,:) = eps(13,:)./5;
p=zeros(num,2);
t=0:2:24;
for n=1:1:num/2
    p(n,:)=polyfit(eps(n,:),g(n,:),1);
    yfit(n,:) =polyval(p(n,:),eps(n,:));
    yresid(n,:)=g(n,:)-yfit(n,:);
    SSresid=sum(yresid(n,:).^2);
    SStotal=(length(g(n,:))-1) * var(g(n,:));
    rsq(n)=1-SSresid/SStotal;
end
for n=1:1:(num/2)
    pt(n)=p(n,1);
    fit(n,:)=(p(n,1)*(0:.2:5) + p(n,2));
end
figure
plot(t,abs(pt))
xlabel('Time (days)','fontsize',18)
ylabel('\alpha','fontsize',18)
figure
title('Change in Frequency vs time')
xlabel('Time (days)')
ylabel('\Delta f/f0')
hold on
for n=1:1:10
    plot(t,g(:,n))
end
legend('20 V','40 V','60 V','80 V','100 V',...
    '120 V','140 V','160 V','180 V','200 V')
hold off
figure
title('Strain vs time')
xlabel('Time (days)')
ylabel('\epsilon')
hold on
```

```
for n=1:1:10
plot(t,eps(:,n))
end
legend('20 V','40 V','60 V','80 V','100 V',...
    '120 V','140 V','160 V','180 V','200 V')
hold off
figure
title('Change in Frequency vs Strain')
xlabel('\epsilon')
ylabel('\Delta f/f0')
hold on
for n=1:1:num/2
    plot(eps(n,:),g(n,:),'-',0:.2:5,fit(n,:),'--')
end
legend('0 Days','2 Days','4 Days','6 Days','8 Days',...
    '10 Days','12 Days','14 Days','16 Days',...
    '18 Days','20 Days','22 Days','24 Days')
hold off
figure
plot(eps(4,:),g(4,:),'-',eps(8,:),g(8,:),'-',eps(12,:),g(12,:),'-',...
    0:.2:5,fit(4,:),'--',0:.2:5,fit(8,:),'--',0:.2:5,fit(12,:),'--')
set(gca,'fontsize',16)
legend('6 Days','14 Days','22 Days','6 Days Linear Fit',...
    '14 Days Linear Fit','22 Days Linear Fit')
xlabel('Induced Strain \epsilon x 10^6','fontsize',18)
ylabel('Relative Frequency Shift \deltaf/f_0','fontsize',18)
grid
for n=2:2:num
    %L=5*.0254; m=.014;S = pi*(5/8/2*.0254)^2;w=2*pi*P(1,1,n-1);
    %young(n/2)=m*w*c(n/2)/tan(w*L/c(n/2))/S;
    rho=8030;
    young(n/2)=rho*c(n/2).^2;
    maxf(n/2)=(P(1,1,n-1)-P(1,37,n))/P(1,1,n-1);
end
```

Bibliography

[1]R.M. Meyer, B. Hanson, and K. Sorenson, "A review of NDE methods for detecting and monitoring of atmospheric SCC in dry cask storage canister for used nuclear fuel," *NACE – Internation Corrosion Conference Series* (2013).

[2]Welding Handbook, 9th ed. Vol 4 (American Welding Society, Miami, 2011), pp. 307-308.

[3]D. Yan, B. W. Drinkwater, and Simon A. Neild, "Experimental and theoretical characterization of kissing bonds in adhesive joint using non-linear ultrasonic measurement," *AIP Conference Proceedings* **1211,** 1190 (2010).

[4]P.A. Johnson, "The new wave in acoustic testing," *Mat. World* **7**, 544-546 (1999).

[5]M. C. Remillieux, R. A. Guyer, C. Payan, and T. J. Ulrich, "Decoupling Nonclassical Nonlinear Behavior of Elastic Wave Type,." *Phys. Rev. Lett.* **116,** 115501 (2016).

[6]K. E.-A.Van Den Abeele, J. Carmeliet, J. TenCate, and P. A. Johnson, "Nonlinear Elastic Wave Spectroscopy (NEWS) techniques to discern material damage. Part II: Single Mode Nonlinear Resonance Acoustic Spectroscopy," *Research on NonDestructive Evaluation* **12**, 31-43 (2000).

[7]J. Rivière, P. Shokouhi, R. A. Guyer, and P. A. Johnson, "A set of measures for the systematic classification of the nonlinear elastic behavior of disparate rocks," *J. Geophys. Res. Solid Earth,* **120**, 1587-1604 (2015).

[8]T. Ohtani and Y. Ishii "Nonlinear Resonant Ultrasound Spectroscopy (NRUS) applied to fatigue damage evaluation in a pure copper," *AIP Conference Proceedings* **1474**, 203 (2012).

[9]T. Ohtani, Y. Kusanagi, and Y. Ishii, "Noncontact nonlinear resonant ultrasound spectroscopy to evaluate creep damage in an austenitic stainless steel," *AIP Conference Proceedings* **1511**, 1227 (2013).

[10]C. Payan, V. Garnier, J. Moysan, and P. Johnson, "Applying nonlinear resonant ultrasound spectroscopy to improving thermal damage assessment," *J. Acoust. Soc. Am.* **121**(4) EL125-EL130 (2007).

[11]C. Payan, T.J. Ulrich, P.Y. Le Bas, T.A. Saleh, M. Guimaraes, "Quantitative Linear and Nonlinear Resonance Inspection Techniques and Analysis for material characterization: Application to concrete thermal damage," *J. Acoust. Soc. Am.* **136**(2), 537-546 (2014).

[12]M. Muller, A. Sutin, R. Guyer, M. Talmant, P. Laugier, and P. A. Johnson, "Nonlinear resonant ultrasound spectroscopy (NRUS) applied to damage assessment in bone," *J. Acoust. Soc. Am.* **118**, 3946-3952 (2005).

[13]Y. Ohara, H. Endo, T. Mihara, and K. Yamanaka, "Ultrasonic measurement of closed stress corrosion crack depth using subharmonic phased array," Japanese J. Appl. Phys. **48**(7S), 07GD01 (2009).

[14]A. Ouchi, A. Sugawara, Y. Ohara, and K. Yamanaka, "Subharmonic phase array for crack evaluation using surface acoustic wave," Japanese J. Appl. Phys. **54**(7S1), 07HC05 (2015).

[15]J. Rivière, M. C. Remillieux, Y. Ohara, B. E. Anderson, S. Haupert, T. J. Ulrich, and P. A. Johnson, "Dynamic Acousto-Elasticity in a Fatigue-Cracked Sample," *J. Nondestruct. Eval.* **33**(2), 216-225 (2014).

[16]Y. Ohara, B.E. Anderson, T. J. Ulrich, P.-Y. Le Bas, P.A. Johnson, and S. Haupert, "Localization of closed cracks using multi-mode nonlinear resonant ultrasound spectroscopy," *J. Japanese Soc. Nondest. Inspec.* **64**(12), 571-578 (2015).

[17]F. Morlock, L. J. Jacobs, J. -Y. Kim, P. Singh, and J. J. Wall, "Nonlinear ultrasonic assessment of stress corrosion cracking damage in sensitized 304 stainless steel," *AIP Conference Proceedings* **1650**, 1641 (2015).

[18]B. E. Anderson, L. Pieczonka, M. C. Remillieux, T. J. Ulrich, and P. -Y. Le Bas, "Stress corrosion crack depth investigation using the time reversed elastic nonlinearity diagnostic," *J. Acoust. Soc. Am.* **141**(1), EL76-EL81 (2017).

[19] L. E. Kinsler, A. R. Frey, A. B. Coppens, and J. V. Sanders, Fundamentals of Acoustics, 4th ed. (Wiley, New York, 2000), pp. 68–87.

[20] S. L. Garrett, Understanding Acoustics (Springer and ASA Press, New York, 2017), Ch. 5, p. 279-305.

[21]T. D. Rossing and D. A. Russell, “Laboratory observation of elastic waves in solids,” *Am. J. Phys.* **58**(12), 1153–1162 (1990).

[22]B. E. Anderson and W. D. Peterson “The song of the singing rod,” *J. Acoust. Soc. Am.* **131**(3), 2435-2443 (2012).

[23]B. K. Jackson, D. A. Bosko, M. T. Cronin, J. L. W. Warwick, and J. J. Wall, “Detection of incipicient SCC damage in primary loop piping using fiber optic strain gages,” *ASME Proceedings of Pressure Vessels and Piping 2014*, PVP2014-28979 (2014).